International Conference on Renewable Energies and Power Quality (ICREPQ'13)
Bilbao (Spain), 20th to 22th March, 2013
Renewable Energy and Power Quality Journal (RE&PQJ)
ISSN 2172-038 X, No.11, March 2013

A novel approach to select HVDC - controller parameters by using a decoupling filter

C. Hahn[1], A. Müller[1] and M. Luther[1]

[1] Chair of Electrical Energy Systems
University of Erlangen – Nuremberg
Konrad-Zuse-Straße 3-5, 91052 Erlangen (Germany)
Phone/Fax number: +49 9131 8523446, e-mail: Christoph.Hahn@ees.fau.de, Annatina-Mueller@web.de, Matthias.Luther@ees.fau.de

Abstract. This paper presents a novel strategy on how to design a sophisticated HVDC controller by using a decoupling filter. At first a simple mathematical model of the HVDC system will be derived. The HVDC is a multivariable system; hence the rectifier and inverter voltages and currents are coupled and therefore it is not trivial to design a controller for one converter station without taking the influence of the opposite converter into account. Subsequently this paper will show how to eliminate this coupling in a mathematical way and as a consequence it will be presented how a controller and its appropriate parameters will be determined. The novel controller will be compared with a standard PI controller of a HVDC system and therefore the dynamic behaviour will be obtained.

Key words

HVDC modelling, control design, decoupling filter, controller parameters.

1. Introduction

Recently the desire to use HVDC systems – especially multiterminal HVDC systems – has gained interest in Germany due to the German grid development plan [1]. Hence the interest in novel control strategies for HVDC systems has increased since the controlling structure design differs from a classical two-point HVDC system, which is shown in Figure 1.

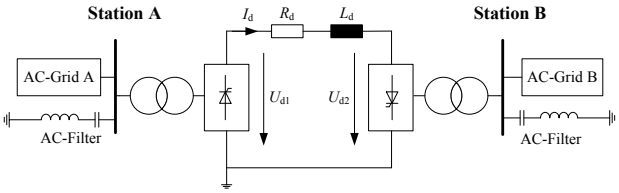

Figure 1: Schematic design of a six pulse HVDC system

The control system plays an important role in the entire HVDC system in order to control the load flow in the AC grids, to minimize losses, to improve the operational behaviour and the system stability, etc. [2]. Usually the rectifier operates in current control mode and the inverter can operate in one of the following control modes: It contains a current controller, a voltage controller and an extinction angle controller [3]. During normal operation, the inverter is in voltage control mode as shown in Figure 2, where $u_d^*(t)$ and $i_d^*(t)$ are the setpoints for the inverter voltage and the rectifier current respectively. $u_d(t)$ and $i_d(t)$ are the actual inverter voltage and rectifier current, α_i and α_r are the firing angles of the inverter and the rectifier respectively.

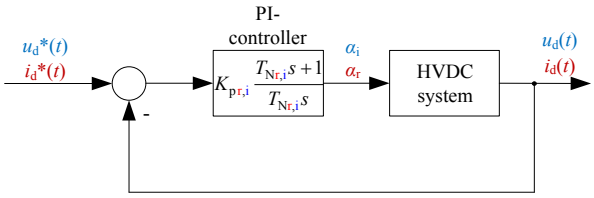

Figure 2: Principle control scheme of an HVDC system during normal operation

Due to AC-Faults at the rectifier side the voltage will drop very fast and the inverter will switch to current control mode in order to prevent that the DC current drops to zero. If the firing angle of the inverter reaches its limitation the inverter switches to extinction angle control mode in order to prevent a tripping of the inverter and the consequently involved risk of a HVDC fall out.
In practice, PI controllers are usually employed to control the rectifier and inverter variables of HVDC systems and approaches already exist to select parameters of these controllers [4], [5]. Also a method for controlling multiterminal HVDC Systems was proposed by F. Karlecik-Maier in 1996 [6].
But typically the controller parameters are obtained by trial and error and therefore this paper will present a method on how to choose a controller and its appropriate parameters in a sophisticated way. It is important to mention that this method will also be applicable to multiterminal HVDC systems due to the decoupling method. At first it will be shown how a simple mathematical model of the HVDC system can be derived.

Afterwards the control design process based on this mathematical model will be shown and the performance of the developed controller will be presented.

2. Modelling of the HVDC system

As already mentioned in the previous section, the first step is to analyse the HVDC system in order to obtain a simple mathematical model. At first the transmission equation can be directly obtained from Figure 1.

$$I_{\mathrm{d}} R_{\mathrm{d}} + L_{\mathrm{d}} \frac{\mathrm{d}\, I_{\mathrm{d}}}{\mathrm{d}\, t} = U_{\mathrm{d1}} - U_{\mathrm{d2}} \tag{1}$$

The voltage drop along the DC line, between the rectifier and inverter, can be replaced by equation (2) and (3), which show the correlation between the DC voltages U_{d1} and U_{d2}, the DC current I_{d}, the firing angle α_{r}, the extinction angle γ_{i} and the corresponding phase to phase voltages of the AC grids U_{nr} and U_{ni} [3].

$$U_{\mathrm{d1}} = B \frac{3\sqrt{2}}{\pi} U_{\mathrm{nr}} \cos\alpha_{\mathrm{r}} - B \frac{3}{\pi} X_{\mathrm{Cr}} I_{\mathrm{d}} \tag{2}$$

$$U_{\mathrm{d2}} = B \frac{3\sqrt{2}}{\pi} U_{\mathrm{ni}} \cos\gamma_{\mathrm{i}} - B \frac{3}{\pi} X_{\mathrm{Ci}} I_{\mathrm{d}} \tag{3}$$

Where X_{Cr} and X_{Ci} are the short-circuit reactances of the AC grids. As the extinction angle γ_{i} is not an actuating variable of the system it can be replaced with its appropriate firing angle α_{i}. For a six-pulse converter the constant B is fixed to one ($B = 1$). Inserting equations (2) and (3) in equation (1) yields equation (4).

$$\begin{aligned} I_{\mathrm{d}} R_{\mathrm{d}} + L_{\mathrm{d}} \frac{\mathrm{d}\, I_{\mathrm{d}}}{\mathrm{d}\, t} = \\ = \frac{3\sqrt{2}}{\pi} \left(U_{\mathrm{nr}} \cos\alpha_{\mathrm{r}} + U_{\mathrm{ni}} \cos\alpha_{\mathrm{i}} \right) - \frac{3}{\pi} \left(X_{\mathrm{Cr}} + X_{\mathrm{Ci}} \right) I_{\mathrm{d}} \end{aligned} \tag{4}$$

This equation describes a nonlinear system and needs to be linearized. This can be done through use of the Taylor series decomposition method, where the differential terms with orders greater than one are neglected. After the linearization the equation can be transferred to the Laplace domain.

$$\begin{aligned} I_{\mathrm{d}}(\mathrm{s}) R_{\mathrm{d}} + \mathrm{s}\, L_{\mathrm{d}} I_{\mathrm{d}}(\mathrm{s}) = -\frac{3\sqrt{2}}{\pi} (U_{\mathrm{nr}} \alpha_{\mathrm{r}}(\mathrm{s}) \sin\alpha_{0\mathrm{r}} + \\ + U_{\mathrm{ni}} \alpha_{\mathrm{i}}(\mathrm{s}) \sin\alpha_{0\mathrm{i}}) - \frac{3}{\pi} (X_{\mathrm{Cr}} + X_{\mathrm{Ci}}) I_{\mathrm{d}}(\mathrm{s}) \end{aligned} \tag{5}$$

$\alpha_{0\mathrm{r}}$ and $\alpha_{0\mathrm{i}}$ are the operating points of the firing angle of the rectifier and the inverter respectively. Hence the transfer function of the DC current can be obtained:

$$\begin{aligned} I_{\mathrm{d}}(\mathrm{s}) = \underbrace{-\frac{\sqrt{2} U_{\mathrm{nr}} \sin\alpha_{0\mathrm{r}}}{\mathrm{s}\frac{\pi}{3} L_{\mathrm{d}} + \frac{\pi}{3} R_{\mathrm{d}} + X_{\mathrm{Cr}} + X_{\mathrm{Ci}}}}_{G_{11}} \alpha_{\mathrm{r}}(\mathrm{s}) - \\ \underbrace{-\frac{\sqrt{2} U_{\mathrm{ni}} \sin\alpha_{0\mathrm{i}}}{\mathrm{s}\frac{\pi}{3} L_{\mathrm{d}} + \frac{\pi}{3} R_{\mathrm{d}} + X_{\mathrm{Cr}} + X_{\mathrm{Ci}}}}_{G_{12}} \alpha_{\mathrm{i}}(\mathrm{s}). \end{aligned} \tag{6}$$

The next step is to deduce the relation between the firing angles and the inverter side DC voltage U_{d2}. Therefore equation (3) will be linearized and transformed to the Laplace domain.

$$U_{\mathrm{d2}}(\mathrm{s}) = \frac{3\sqrt{2}}{\pi} U_{\mathrm{ni}} \alpha_{\mathrm{i}}(\mathrm{s}) \sin\alpha_{0\mathrm{i}} - \frac{3}{\pi} X_{\mathrm{Ci}} I_{\mathrm{d}}(\mathrm{s}) \tag{7}$$

Replacing the DC current I_{d} in equation (7) with (6) yields equation (8).

$$\begin{aligned} U_{\mathrm{d2}}(\mathrm{s}) = \\ = \underbrace{\frac{3\sqrt{2}}{\pi} U_{\mathrm{ni}} \sin\alpha_{0\mathrm{i}} \frac{\mathrm{s}\frac{\pi}{3} L_{\mathrm{d}} + \frac{\pi}{3} R_{\mathrm{d}} + X_{\mathrm{Cr}}}{\mathrm{s}\frac{\pi}{3} L_{\mathrm{d}} + \frac{\pi}{3} R_{\mathrm{d}} + X_{\mathrm{Cr}} + X_{\mathrm{Ci}}}}_{G_{22}} \alpha_{\mathrm{i}}(\mathrm{s}) \\ \underbrace{-\frac{3\sqrt{2}}{\pi} U_{\mathrm{nr}} \sin\alpha_{0\mathrm{r}} \frac{X_{\mathrm{Ci}}}{\mathrm{s}\frac{\pi}{3} L_{\mathrm{d}} + \frac{\pi}{3} R_{\mathrm{d}} + X_{\mathrm{Cr}} + X_{\mathrm{Ci}}}}_{G_{21}} \alpha_{\mathrm{r}}(\mathrm{s}) \end{aligned} \tag{8}$$

Summarizing equation (6) and (8) yields in the transfer matrix **G**.

$$\begin{pmatrix} I_{\mathrm{d}}(\mathrm{s}) \\ U_{\mathrm{d2}}(\mathrm{s}) \end{pmatrix} = \underbrace{\begin{pmatrix} G_{11} & G_{12} \\ G_{21} & G_{22} \end{pmatrix}}_{\mathbf{G}} \begin{pmatrix} \alpha_{\mathrm{r}}(\mathrm{s}) \\ \alpha_{\mathrm{i}}(\mathrm{s}) \end{pmatrix} \tag{9}$$

As the transfer matrix shows, the model is a two-variable system where all the variables are influenced by each other. The structure of the system is shown in Figure 3.

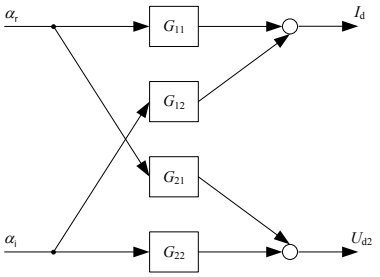

Figure 3: Structure of the simplified HVDC Model

It is not possible to design an appropriate controller for such a system due to the fact that both, actuating and control variables, are coupled. Applying a so called decoupling filter to the system makes it possible to consider the coupled system mathematically decoupled [7]. The filter compensates the influence of the secondary diagonal elements G_{12} and G_{21}. Its matrix is shown in equation (10).

$$\mathbf{F} = \begin{pmatrix} F_{11} & F_{12} \\ F_{21} & F_{22} \end{pmatrix} \tag{10}$$

The structure of the system with the applied filter and the controllers C_{11} and C_{22} is shown in Figure 4.

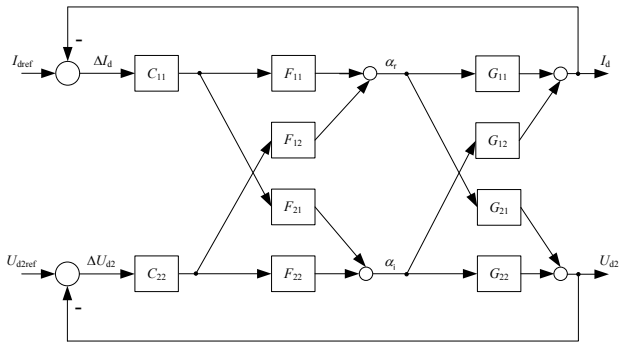

Figure 4: Structure of the HVDC system with inculded filter and controllers

The controllers C_{11} and C_{22} and its parameters are a degree of freedom and can be selected in order to guarantee a certain dynamic behaviour of the HVDC system. Selecting the filter parameters in the right way, the system can be considered completely decoupled and has a structure as shown in Figure 5.

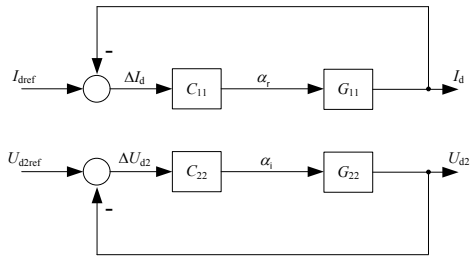

Figure 5: Structure of the HVDC system with the applied decoupling filter

The first step in the creation of the filter matrix is to reveal the undesired influence of the DC current I_d on the inverter end DC voltage U_{d2} and to zero it in.

$$\Delta I_d C_{11}\left(F_{21}G_{22} + F_{11}G_{21}\right) = 0 \tag{11}$$

$$\Delta U_{d2} C_{22}\left(F_{12}G_{11} + F_{22}G_{12}\right) = 0 \tag{12}$$

Solving these equations yields in the following expressions for the secondary diagonal elements of the decoupling filter:

$$F_{12} = -\frac{G_{12}}{G_{11}}F_{22}, \tag{13}$$

$$F_{21} = -\frac{G_{21}}{G_{22}}F_{11}. \tag{14}$$

The direct influences from the input to the output, shown in Figure 4, shall remain and therefore the equations can be presented.

$$I_d = \Delta I_d C_{11}\left(F_{21}G_{12} + F_{11}G_{11}\right) \tag{15}$$

$$U_{d2} = \Delta U_{d2} C_{22}\left(F_{12}G_{21} + F_{22}G_{22}\right) \tag{16}$$

Comparing those to the decoupled structure scheme, shown in Figure 5, yields in the following equations:

$$G_{11} = F_{21}G_{12} + F_{11}G_{11}, \tag{17}$$

$$G_{22} = F_{12}G_{21} + F_{22}G_{22}. \tag{18}$$

Inserting equation (13) in (17) and equation (14) in (18) respectively and solving the equations for F_{11} or F_{22} respectively one obtains equation (19).

$$F_{11} = F_{22} = \frac{G_{11}G_{22}}{G_{11}G_{22} - G_{12}G_{21}} \tag{19}$$

Hence the decoupling filter matrix is given through equation (20).

$$\mathbf{F} = \frac{G_{11}G_{22}}{G_{11}G_{22} - G_{12}G_{21}} \begin{pmatrix} 1 & -\frac{G_{12}}{G_{11}} \\ -\frac{G_{21}}{G_{22}} & 1 \end{pmatrix} \tag{20}$$

The system can now be considered as a mathematically uncoupled system and control design can be applied much easier.

3. Control Design

For designing a sophisticated controller for the HVDC system, a simple test network was build up in MATLAB® Simulink® with some standard values for Back-to-Back HVDC systems from [4] and [8], shown in Table I.

Table I - HVDC Values

U_{nr}	200 kV
U_{ni}	200 kV
X_{cr}	0,7 Ω
X_{ci}	0,7 Ω
R_d	0,1 Ω
L_d	0,085H
U_{d2ref}	255 kV
I_{dref}	3000 A
α_{0r}	10°
α_{0i}	160°

The transfer functions of the G_{11} and G_{22} of the decoupled system can now be presented in equation (21) and (22).

$$G_{11} = \frac{-3,264 \cdot 10^4}{0.05916\,\mathrm{s}+1} \tag{21}$$

$$G_{22} = 4,94 \cdot 10^4 \frac{0.11063\,\mathrm{s}+1}{0.05916\,\mathrm{s}+1} \tag{22}$$

Figure 6 shows the bode chart of the transfer function of $-G_{11}$ (blue) and G_{22} (green).

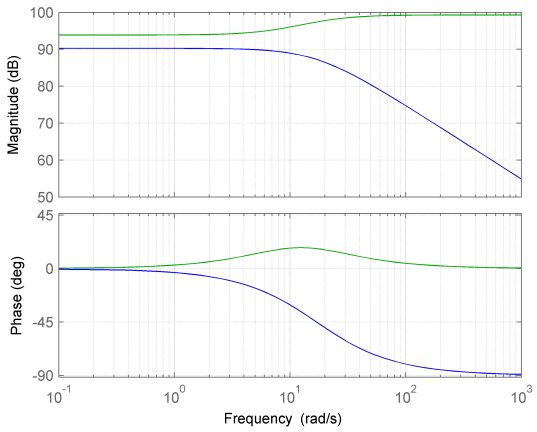

Figure 6: Bode chart of the transfer function $-G_{11}$ (blue) and G_{22} (green)

G_{11} shows delay first order behaviour with a negative gain. The negative sign of G_{11} is not taken into account for further studies since the control direction is simply adapted with a negative sign in the controller gain. G_{22} is a PDT1 element.
The next two sections will show how control design is applied for the mathematically separated systems G_{11} and G_{22}.

A. Control design for G_{11}

Since the transfer functions G_{11} is already pretty fast due to its large gain crossover frequency, it is sufficient to use a PI controller, which will handle the steady-state accuracy. The equation of a PI controller is shown in (23).

$$C_{11} = K_\mathrm{p} \frac{1+T_\mathrm{N}\,\mathrm{s}}{T_\mathrm{N}\,\mathrm{s}} \tag{23}$$

Where K_p is the gain and T_N is the time constant of the PI controller. The time constant of the PI controller is chosen in order to eliminate the pole in the transfer function G_{11}. The gain of the controller has to be chosen in order to guarantee a certain dynamic behaviour. A limiting factor is the firing delay of 60° on average. The firing frequency can be calculated as shown in equation (24).

$$\omega_\mathrm{f} = 2\pi \frac{360° \cdot 50\,\mathrm{Hz}}{60°} = 1885\,\mathrm{rad/sec} \tag{24}$$

If the controller provides a lower gain crossover frequency than ω_f the DC current control is delayed. Hence the gain was chosen to $K_\mathrm{p} = -0{,}006$ in order to exceed this limiting value for the open loop gain crossover frequency and to adapt the control direction with the negative sign. Consequently the DC current controller has the following structure:

$$C_{11} = -0.006 \frac{1+0.05916\,\mathrm{s}}{0.05916\,\mathrm{s}}. \tag{25}$$

Figure 7 shows the bode chart of the closed loop system and it can be easily seen that the system is speeded up.

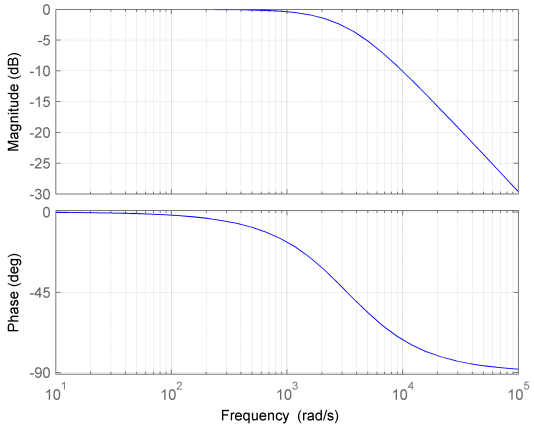

Figure 7: Bode chart of the closed loop system $C_{11} \cdot G_{11}$

B. Control design for G_{22}

As already mentioned G_{22} is described by a PDT2 element, which is similar to an all-pass filter. This means, that all frequencies are barely damped. Therefore also PDT2 controller can be deployed where the equation is presented in (26).

$$C_{22} = K_\mathrm{p} \frac{(1+T_\mathrm{N}\,\mathrm{s})}{T_\mathrm{N}\,\mathrm{s}(1+T_\mathrm{V}\,\mathrm{s})} \tag{26}$$

The time constants T_N and T_V of the PDT2 controller are chosen in order to eliminate the pole in the transfer function G_{22} and the zero respectively. Hence the closed loop transfer function is described by a delay first order element. Therefore the gain of the PDT2 controller can be chosen in order to guarantee a fast dynamic response as well as a sufficiently damped transient behavior. The gain was set to $K_\mathrm{p} = 0{,}006$. Hence the appropriate PDT2 controller C_{22} can be presented in equation (27).

$$C_{22} = 0,006 \frac{1+0.05916\,\mathrm{s}}{0.05916\,\mathrm{s}(1+0.11063\,\mathrm{s})} \tag{27}$$

The bode plot of the closed loop system is shown in Figure 8. It can also be seen that the system is speeded up.

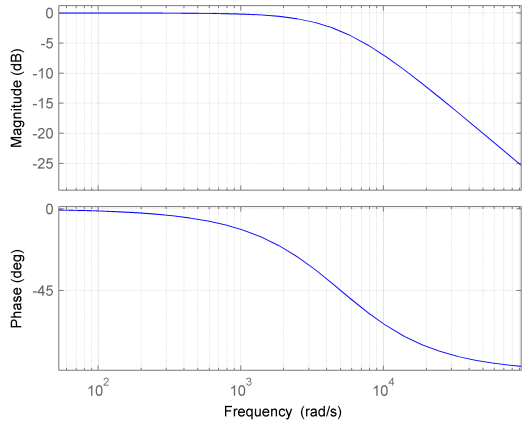

Figure 8: Bode chart of the closed loop system $C_{22} \cdot G_{22}$

4. Results

In this section the results of the aforementioned control design process will be presented. Therefore the novel approach will be compared with a classical HVDC control scheme. This comparison will include normal operating conditions as well as operation during fault conditions. The classical HVDC controller consists of two controllers, a PI controller at the rectifier end for the DC current and a PI controller at the inverter end for the DC voltage. Therefore standard HVDC PI parameters are considered and shown in Table II.

Table II: Parameters of standard HVDC PI controllers [4]

PI at rectifier side		PI at inverter side	
K_p	T_N	K_p	T_N
0,4	0,015 sec.	0,2	0,02 sec

A. No fault operation

The first simulation shows a power-up process of the HVDC system with the different controllers deployed; it is presented in Figure 9.
It is very conspicuous that the decoupling filter controller is much faster than the classical controller. It reaches its reference level for the DC voltage approximately four times faster than the classical controller. In order to achieve this goal one has to accept overshoots in the DC current.

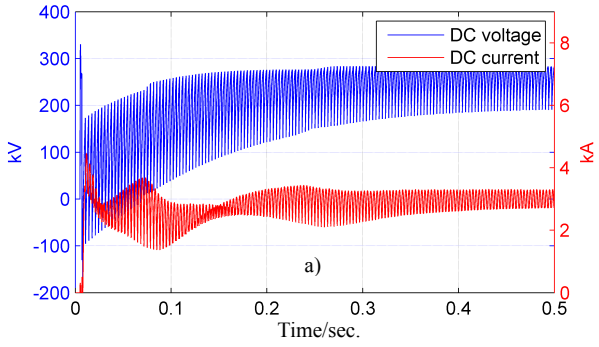

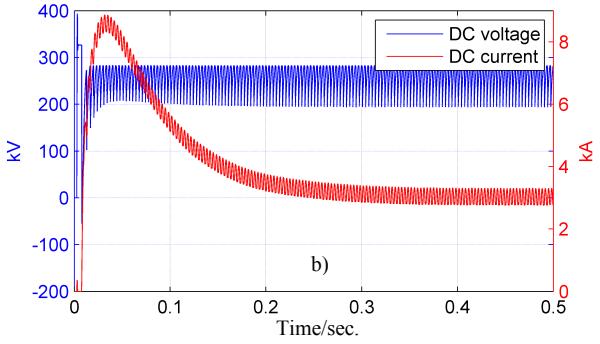

Figure 9: Power-up process of the HVDC system with a) the classical controller b) the decoupling filter controller

This behaviour differs from the predicted delay first order; the reason is a simplification in the system model. As already mentioned the HVDC is a nonlinear system due to the sinusoidal dependence of the system variables on the firing angle and also due to the firing delay of 60° on average [9]. This firing delay is equal to a dead-time element. During this interval of 60° the HVDC is not capable to interact and therefore the overshoot arises. The transfer function of such a dead-time element can be described as follows.

$$F_t(s) = e^{-T_t s} \tag{28}$$

Another positive impact is the smoothness of the firing angels, which implies that there aren't any additional filters for the DC current and voltage values in the controlling software required; the firing angles are presented in Figure 10.

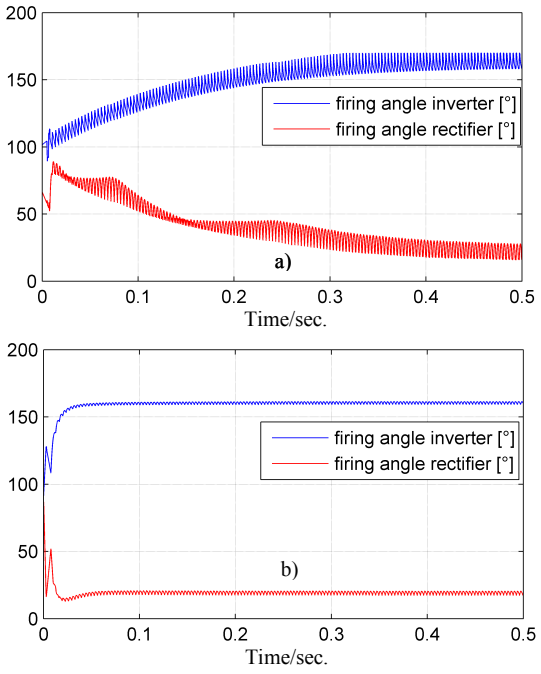

Figure 10: Firing angles of the HVDC system with a) the classical controller b) the decoupling filter controller

B. Operation during AC faults

The AC fault applied to the HVDC system is a 50% voltage jump at the AC side of the inverter; it is presented in Figure 11.

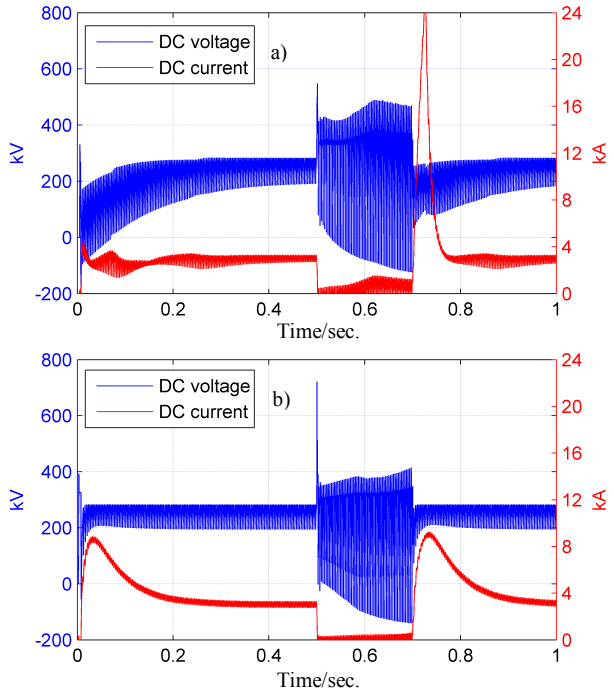

Figure 11: 50 % voltage jump from $t = 0.5$ sec to $t = 0.7$ sec applied to the inverter AC side of the HVDC system with a) the classical controller b) the decoupling filter controller

During the AC fault, the rectifier firing angle decreases and is controlled to its average reference value. The DC current drops to zero. Applying the classical control the current overshoot after the fault is much higher than applying the decoupling filter controller. The decoupling filter reacts much faster than the classical controller and reaches its reference level much earlier regarding the DC voltage.

5. Conclusion

In this paper a novel approach for the selection of HVDC controller parameters was presented. First the mathematical modelling of an HVDC was shown, thus it was revealed that the HVDC is a coupled system due to the firing of the rectifier influences the DC current and the DC voltage at the inverter; the same applies for the firing of the inverter respectively and was presented in Figure 3.

Accordingly a decoupling filter was designed for the HVDC system and it was shown, that the system can be considered as mathematically uncoupled.

This method offers the possibility to select the HVDC controllers and their parameters in a sophisticated way that takes the HVDC parameters of the mathematical model into account. Therefore an appropriate controller for each HVDC system can be designed; unlike the parameters of classical controllers which were obtained by trial and error.

The controller was tested in a realistic environment and it was shown, that the developed controller operates well and that it behaves even better under certain operating conditions than the classical HVDC controller.

It was also shown that the curves of the firing angles are very smooth, therefore no additional software smoothing filters would be necessary in the controller like it is necessary for the classical controller.

References

[1] O. Feix, R. Obermann, M. Strecker and A. Brötel, “German grid development plan, (Netzentwicklungsplan Strom)“, German Transmission System Operators, Berlin, Germany, August 2012 (in German).

[2] L. Ni and Y. Tao, “Parameter Optimization of the Control and Regulating System of Gezhouba-shanghai HVDC Project”, Power System Technology, No.3, pp.26-31, Aug. 1989.

[3] V. Crastan and D. Westermann, “Electrical power supply III, (Elektrische Energieversorgung III)”, Springer publishing, Berlin Heidelberg, Germany, 2012 (in German).

[4] F. Yang and Z. Xu, “An approach to Select PI Parameters of HVDC Controllers”, Power Engineering Society General Meeting, Montreal, Québec, Canada, June 2006.

[5] A. E. Hammad, “Stability and Control of HVDC and AC Transmissions in Parallel”, IEEE Transactions on Power Delivery, Vol. 14, No. 4, October 1999.

[6] F. Karlecik-Maier, “A New Closed Loop Control Method for HVDC Transmission”, IEEE Transactions on Power Delivery, Vol. 11, No. 4, October 1996.

[7] O. Föllinger, “Control Engineering, (Regelungstechnik)”, Hüthig publishing, Heidelberg, Germany, 1994 (in German).

[8] T. Rae, E. Boje, G. D. Jennings and R. G. Harley, “Controller structure and design of firing angle controllers for (unit connected) HVDC systems”, 4th IEEE Africon Conference, Stellenbosch, South Africa, September 1996.

[9] C. Hahn, M. Weiland, G. Herold, “Control design for a power electronic based fault current limiter (FCL)”, International Conf. on Renewable Energies and Power Quality (ICREPQ), Santiago de Compostela (Spain), 2012.